

The surface of the empirical horopter

Kai M. Schreiber

School of Optometry, University of California at Berkeley,
CA, USA



James M. Hillis

Department of Psychology, University of Glasgow,
Glasgow, UK



Heather R. Filippini

UCSF/UC Berkeley Joint Graduate Group in Bioengineering,
University of California at Berkeley,
CA, USA



Clifton M. Schor

School of Optometry, University of California at Berkeley,
CA, USA



Martin S. Banks

School of Optometry, Psychology, Wills Neuroscience,
University of California at Berkeley, CA, USA



The distribution of empirical corresponding points in the two retinas has been well studied along the horizontal and the vertical meridians, but not in other parts of the visual field. Using an apparent-motion paradigm, we measured the positions of those points across the central portion of the visual field. We found that the Hering–Hillebrand deviation (a deviation from the Vieth–Müller circle) and the Helmholtz shear of horizontal disparity (backward slant of the vertical horopter) exist throughout the visual field. We also found no evidence for non-zero vertical disparities in empirical corresponding points. We used the data to find the combination of points in space and binocular eye position that minimizes the disparity between stimulated points on the retinas and the empirical corresponding points. The optimum surface is a top-back slanted surface at medium to far distance depending on the observer. The line in the middle of the surface extending away from the observer comes very close to lying in the plane of the ground as the observer fixates various positions in the ground, a speculation Helmholtz made that has since been misunderstood.

Keywords: stereo vision, stereopsis, horopter, correspondence

Citation: Schreiber, K. M., Hillis, J. M., Filippini, H. R., Schor, C. M., & Banks, M. S. (2008). The surface of the empirical horopter. *Journal of Vision*, 8(3):7, 1–20, <http://journalofvision.org/8/3/7/>, doi:10.1167/8.3.7.

Introduction

Retinal correspondence and the horopter

In stereopsis, the visual system must first match points in the two retinal images that correspond to the same point in space. The difficulty of solving this matching problem is highlighted by the fact that for every n points in an image there are n^2 possible matches, which becomes a very large number with complex stimuli such as random-element stereograms (Julesz, 1971). One part of the solution to this problem is the existence of points in the two retinas with a special physiological relationship: For each point in one retina, there is a point in the other that when stimulated gives rise to the same perceived direction (i.e., the points appear superimposed in visual space). These pairs, which are called *corresponding points*, have special status for binocular vision: (1) matching solutions between the two eyes' images are biased toward them

(Brewster, 1844; Prince & Eagle, 2000); (2) the region of single vision straddles them (Fischer, 1924); and (3) the precision of depth estimates from disparity is highest for locations in space that project to those points (Badcock & Schor, 1985; Blakemore, 1970; Breitmeyer, Julesz, & Kropfl, 1975; Ogle, 1953; Schumer & Julesz, 1984; Westheimer, 1982). We measured the locations of corresponding points across the central visual field and used the measurements to estimate the shape of the surface for which human stereopsis is best suited. Such information provides important insight into how stereopsis functions in the natural environment. It can also be used to design workstations that maximize visual performance and reduce viewer fatigue (Ankrum, Hansen, & Nemeth, 1995).

To quantify the locations of corresponding points, one typically measures the angles between retinal points and the foveae; we use Helmholtz coordinates to do so (in Helmholtz coordinates, elevation is assessed relative to the eye's horizontal plane and azimuth is assessed in the elevated plane; Fig. 20.1c, Howard & Rogers, 2002).

There are two types of corresponding points: geometric and empirical. Geometric corresponding points are points with the same coordinates in the two retinas; they are thus defined mathematically. Empirical corresponding points are located by experimental measurement, so they are defined by psychophysical or physiological criteria. Both types of corresponding points are fixed retinally: geometric points by definition and empirical points by experimental demonstration (Hillis & Banks, 2001). Much research has been devoted to determining the positions of empirical corresponding points along the eyes' horizontal or vertical meridians. All have found that empirically measured corresponding points are not coincident with geometric corresponding points (Helmholtz, 1925; Hillis & Banks, 2001; Nakayama, 1977; Ogle, 1950).

The set of locations in space that project onto corresponding retinal points is the *horopter* (Helmholtz, 1925; Howard & Rogers, 2002; Tyler, 1991). The geometric horopter is constructed by projecting rays out of the eyes from pairs of geometric corresponding points and finding the intersections of those rays; only a subset of rays yields intersections and the positions of the intersections obviously depend on eye position (Figure 1). The empirical horopter is constructed by projecting rays from empirical corresponding points; again only a subset yields intersections and again the intersection positions depend on eye position.

The geometric horopter generally contains two parts: the Vieth–Müller circle (the circle containing the fixation point and the eyes' nodal points) and a vertical line that lies in the head's mid-sagittal plane and intersects the Vieth–Müller circle. In fact, the statement that the geometric horopter is a circle and a vertical line depends on eye position: The eyes must be fixating such that either Helmholtz torsional vergence (the difference between the two eyes' torsional positions in Helmholtz coordinates) or horizontal version (the average of their horizontal positions) are zero; when both are different from zero, the geometric horopter becomes a spiral (Schreiber, Tweed, & Schor, 2006).

Empirical corresponding points are usually determined using a nonius criterion: For a fixed eye position, a point

or line presented to one eye is moved horizontally and/or vertically until it is perceived in the same direction as a point or line in the other eye (Ogle, 1932). The resulting pairs are empirical corresponding points. Relative to geometric points, empirical points have uncrossed horizontal disparities to the left and right of fixation, so the empirical horizontal horopter (the part that lies in the visual plane) is less concave than the Vieth–Müller circle. This difference with respect to the Vieth–Müller circle is the *Hering–Hillebrand deviation* (e.g., Ames, Ogle, & Gliddon, 1932; Ogle, 1932; Shipley & Rawlings, 1970; see Equation 1). Because the retinal positions of empirical corresponding points do not shift with eye movements (Hillis & Banks, 2001), the Hering–Hillebrand deviation remains constant when expressed in angular units. However, the curvature of the empirical horizontal horopter changes with vergence eye movements because of the relationship between disparity and distance (Howard & Rogers, 2002; Ogle, 1950). With decreasing vergence (increasing distance), it becomes less concave and eventually becomes convex. Relative to geometric corresponding points, empirical corresponding points near the vertical meridians of the retinas are sheared horizontally such that uncrossed disparities are required to stimulate corresponding points above the fovea and crossed disparities below, and the magnitude of these disparities increases linearly with elevation. This vertical gradient of horizontal disparity has been called the *Helmholtz shear*. It causes a top-back slant of the vertical horopter (Helmholtz, 1925; Nakayama, 1977; Siderov, Harwerth, & Bedell, 1999; Tyler, 1991). Because of the relationship between disparity and distance, the slant of the empirical vertical horopter increases with fixation distance.

Rays from geometric corresponding points that are not on the horizontal or vertical meridians of the retinas will generally not intersect. The red and green rays illustrated in Figure 1 are examples of such non-intersecting rays. Thus, there is no location in space that could stimulate such a pair of points. This is true of most pairs of corresponding points, so as we said earlier the geometric horopter is generally restricted to a circle and a line. Likewise, many empirical corresponding points may not

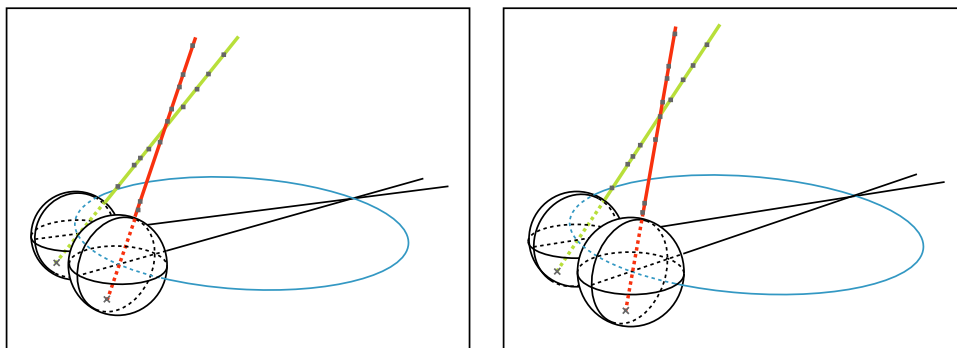


Figure 1. Stereogram showing ray projections for a pair of geometric corresponding points. The eyes are converged at 15° . The green ray is projected from $(-40^\circ, 20^\circ)$ in the left eye and the red ray from $(-40^\circ, 20^\circ)$ in the right eye. The two rays do not intersect.

have a real-world horopter if the strict definition of the horopter—the intersection of rays from corresponding points—is used. We can, however, relax the definition to include the points in space that project closest to pairs of empirical corresponding points, as quantified by the magnitude of the total disparity angle irrespective of the retinal direction of this angle (Schreiber et al., 2006). With this definition, the horopter is a 3D surface for all eye positions and distributions of corresponding points. We will use this relaxed definition—the minimum-disparity horopter—to describe the empirical horopter.

The fact that empirically measured corresponding points are not geometric corresponding points suggests that the positions of empirical points may be optimized for a particular surface shape and orientation that is advantageous behaviorally. For example, the combination of the Hering–Hillebrand deviation near the horizontal meridian and the Helmholtz shear near the vertical meridian has led to the speculation that empirical corresponding points are optimized for a ground plane viewed by a standing observer (Breitmeyer, Battaglia, & Bridge, 1977; Helmholtz, 1925; Nakayama, 1977; Tyler, 1991). A similar shear exists in cats and owls, and the shear magnitudes correlate with those species' habitual heights above the ground (Cooper & Pettigrew, 1979). If the empirical horopter coincides with the ground plane, we would expect a pattern of disparities that mimics the back projection of a slanted plane on the retinas. The horizontal and vertical disparities of empirical corresponding points throughout the retinas should both follow this pattern.

Similarly, the distribution of empirical corresponding points may be optimized for a particular eye position that is advantageous behaviorally. With natural eye movements (i.e., eye movements that follow Listing's law or Listing's extended law; Mok, Ro, Cadera, Crawford, & Vilis, 1992; Tweed, 1997; Van Rijn & Van den Berg, 1993), the only pair of fixed retinal points whose projections will always intersect are the foveae. Therefore, with empirical corresponding points that are fixed on the retinas (Hillis & Banks, 2001), there may be only one eye position for which points in space on the most appropriate surface (perhaps a top-back slanted plane) come closest to stimulating empirical points throughout the retinas. We can express the combination of surface properties and eye position that comes closest to stimulating empirical corresponding points by the shape, orientation, and 3D position of the surface. We will call this the *optimum surface* because it is the surface for which the precision of stereopsis should be highest.

To determine what the optimum surface is, we need to know the distribution of empirical corresponding points across the retinas, not just in the horizontal and vertical meridians, and then we need to find the combination of binocular eye position and point positions in space that minimizes the disparity between stimulated retinal points and empirical corresponding points. To our knowledge, only two published papers have reported measurements of

corresponding point locations off the horizontal and vertical meridians: Ledgeway and Rogers (1999) and Grove, Kaneko, and Ono (2001). Their data suggest that the Helmholtz shear observed along the vertical meridian extends to a large portion of the visual field. Their data also suggest that there is little if any vertical disparity between corresponding points. They did not, however, determine the optimum surface. Furthermore, their psychophysical method measured only global components of disparity between corresponding points (with the exception of the measurements of horizontal disparities by Grove et al., 2001). There is also an unpublished manuscript that made measurements of corresponding point locations off the major meridians (Owens, Kooi, & Tyler, 1987), but we do not know the details of their method.

We measured the pattern of retinal correspondence over the central portion of the visual field using a technique that allowed us to measure global and local variation in the disparities of corresponding points. We then used those measurements to find the combination of binocular eye position and points in space that minimizes the overall disparity between stimulated points and empirical corresponding points. From this, we derived the optimum surface.

Methods

Observers

There were three observers ranging in age from 23 to 30 years. All had normal stereopsis and retinal correspondence assessed by the Randot stereotest. HRF has a modest intermittent exophoria (8°) and received eye exercises to enhance convergence amplitudes in childhood (age 8–10 years). Her correspondence was assessed and found to be normal using the Hering–Bielschowsky after-image test; her eye alignment was assessed and found to be normal using the unilateral cover test at 40 and 600 cm. Two of the observers were authors; PRM was unaware of the specific experimental hypotheses. The experimental measurements were quite difficult, so all observers had extensive practice before beginning formal testing.

Apparatus

The stimuli were displayed on a haploscope with two mirrors and two CRTs (one mirror and CRT for each eye; for details, see Backus, Banks, van Ee, & Crowell, 1999). Each mirror and CRT was attached to an arm that rotated about a vertical axis. Observers were positioned with a bite bar so that the vertical rotation axes of their eyes were co-linear with the rotation axes of the haploscope arms. With this arrangement, the line of sight from each eye was

co-linear with the central surface normal of the corresponding CRT. To position the observer's eyes relative to the bite-bar mount, we used a sighting device described by Hillis and Banks (2001). The optical distance from the eye centers to the CRTs was 39 cm. The arms of the haploscope were rotated such that the vergence distance was 40 cm; this required adjusting the distance between the rotation axes of the two arms so that they were an interocular distance apart. Because the vergence and the optical distances were so similar, there was very little conflict between the stimuli to vergence and accommodation (Judge & Miles, 1985).

Stimulus and procedure

Several methodological challenges had to be overcome for the psychophysical measurements. Variation in eye position from one trial to the next would cause undue variability in the observers' settings, so one challenge was to hold eye position as constant as possible across trials. To help achieve this, we presented a fixation target that allowed observers to assess their own fixation accuracy before initiating a trial. The fixation target was composed of several line segments in a radial pattern (Figure 2). The central part of the target was a three-segment radial pattern presented binocularly; the segments were 0.34 cm (0.5°) long. Observers were instructed to fixate the center of this pattern. The eccentric part of the fixation target was a radial pattern of segments each abutting the end of a segment in the central binocular part of the target; these segments were also each 0.5° long and were presented dichoptically, three to the left eye and three to the right. Observers were instructed to keep the radial segments aligned and in particular to initiate stimulus presentations only when they were aligned. Empirical corresponding points are fixed retinally (Hillis & Banks, 2001), so the dichoptic segments would have appeared unaligned if the observer was not fixating accurately.

While torsion is normally determined by the binocular extension of Listing's law during stable fixation, small fluctuations occur around the prescribed value (Van Rijn, Van der Steen, & Collewijn, 1994). To help keep the eyes torsionally aligned, we presented eight binocular line segments in between each stimulus presentation. Each segment was 13 cm ($\sim 8^\circ$) long; segment orientations were radial with respect to the fixation target (Figure 2). Observers were encouraged to maintain fusion of these segments, which required the torsional vergence to be close to 0° .

The test stimuli were 15-mm vertical or horizontal dichoptic line segments (corresponding to $\sim 0.22^\circ$). They were anti-aliased so we were able to adjust their positions with an accuracy of 0.3 arcmin or better (Backus et al., 1999). The vertical segments were used for measuring horizontal disparities in empirical corresponding points and the horizontal segments for measuring vertical disparities. The stimuli were presented at seven eccentricities from

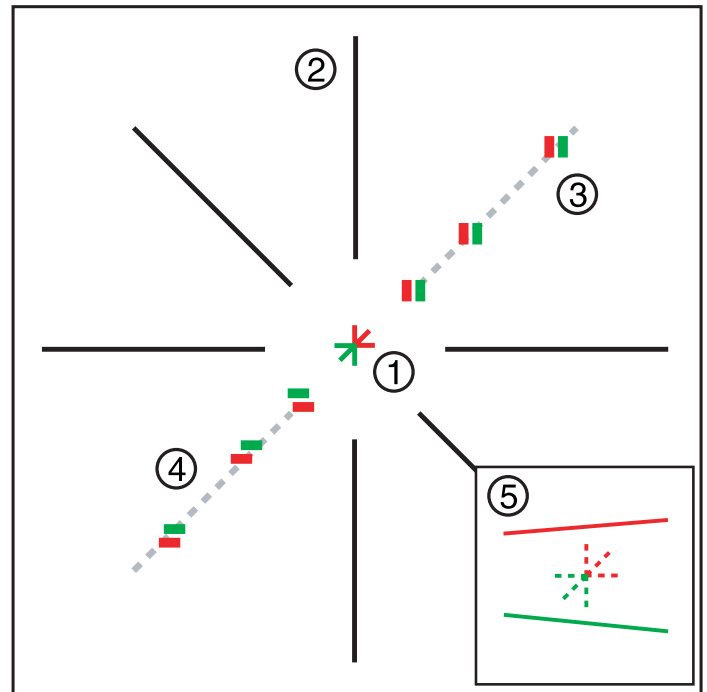


Figure 2. Stimulus schematic showing (1) the central fixation target, a dichoptic star; (2) the background fixation target; (3) the stimulus geometry for determination of horizontal disparities of empirical corresponding points; and (4) the stimulus geometry for determination of vertical disparities. (5) The inset shows the stimulus used to measure torsional vergence. Red components were seen by the right eye, green by the left eye. See [Methods](#) section for full stimulus description.

fixation (0° , $\pm 2^\circ$, $\pm 4^\circ$, and $\pm 8^\circ$; 0° was used to measure fixation disparity) along one of eight radial directions (0° , 22.5° , 45° , 67.5° , 90° , 112.5° , 135° , and 157.5° , where 0° is horizontal). The seven possible stimulus locations are shown in Figure 2 for the 45° direction. Two limbs of the radial background pattern were extinguished during the presentation of the test stimuli if they overlapped the position of the test stimulus.

In each experimental session, we measured horizontal and vertical disparities between corresponding points for seven eccentricities (including fixation) along one radial meridian. We first measured horizontal disparities for all seven eccentricities. On each trial, the stimuli could appear at any one of the seven eccentricities. The random selection of eccentricity was important because it prevented observers from making anticipatory eye movements toward the test location. On each trial, dichoptic vertical line segments, one in the left eye and one in the right, were flashed sequentially for 55 ms each, separated by 70 ms. The two segments were offset horizontally (in screen coordinates) in opposite directions from the test location. The eye stimulated first was selected randomly. This sequential dichoptic presentation yielded apparent horizontal motion unless the segments stimulated corresponding points (Flom, 1980; Ledgeway & Rogers, 1999;

Nakayama, 1977). Observers indicated the direction of apparent motion from the two flashes. The offsets were varied trial by trial with a 1-up/1-down adaptive staircase, with six step-size reductions after each of the first six reversals of staircase direction. Each staircase terminated after 12 reversals. The ending step sizes were 0.3 arcmin for 0° eccentricity and 0.5 arcmin for the others. Seven staircases—one for each of the eccentricities along the chosen meridian—were interleaved. When each staircase ended, we estimated the horizontal disparity associated with each tested eccentricity by fitting the data with a cumulative Gaussian using a maximum-likelihood criterion (Wichmann & Hill, 2001). The estimated disparity at each eccentricity was the mean of the best-fitting cumulative Gaussian. These horizontal-disparity estimates were then used to position the horizontal dichoptic lines used to measure vertical disparities associated with corresponding points.

We used the same task to measure vertical disparities except that observers now indicated whether apparent motion was up or down. Seven interleaved staircases were used to vary the vertical disparity at each eccentricity along the chosen meridian. These vertical-disparity measurements yielded the vertical locations of empirical corresponding points. Once the horizontal and the vertical locations were estimated, the observer should have perceived no apparent motion when targets were flashed at the appropriate locations in the two eyes.

Throughout the paper, horizontal disparity refers to the difference in the azimuths of left- and right-eye positions expressed in Helmholtz coordinates; vertical disparity refers to the difference in the Helmholtz elevations. We also define rightward (i.e., clockwise) horizontal angles as positive because Ogle (1950) used that sign convention. We define upward vertical angles as positive.

The psychophysical judgments were very difficult, particularly at the 8° eccentricity, but after several modifications of the time, the segment length, and the other details, we were able to obtain repeatable settings for all 49 of the tested positions in the visual field.

Subjective measures of eye position

Despite the instructions and fixation aids, there is no assurance that observers fixated the central target perfectly; that is, that the horizontal, the vertical, and the torsional vergence was zero. With the physical constraints of the haploscope, we were unable to measure eye position objectively with an eye-movement recorder. So to measure any residual fixation errors, we measured vergence subjectively during the course of the experiment and used the measurements to correct the corresponding-point data. Previous work has shown that the nonius technique we used yields accurate estimates of horizontal, vertical, and torsional vergence (Hebbard, 1962; Howard, Ohmi, & Sun, 1993; Shipley & Rawlings, 1970).

The stimuli for measuring vergence were varied according to 1-up/1-down staircases; this is one of the aforementioned seven staircases. For measurements of horizontal vergence, dichoptic vertical segments were presented at 0° eccentricity and their relative positions were varied horizontally. On each trial, observers indicated which segment appeared farther to the right. For measurements of vertical vergence, horizontal segments were presented and their relative positions were varied vertically. Observers indicated which segment appeared higher in the visual field. For measurements of torsional vergence, two 2-cm line segments were presented, one 0.3 cm above the fixation target and one 0.3 cm below. Observers indicated whether the upper segment was rotated clockwise or counterclockwise relative to the lower. We used these dichoptic alignment tasks rather than the apparent-motion task we used at the other eccentricities because observers were able to make more alignment judgments near fixation.

The trials for measuring horizontal, vertical, and torsional vergence were randomly interspersed with the other measurements, so eye alignment during the vergence measurements should have been the same as during the corresponding-point measurements. The data were used to generate psychometric functions fit by cumulative Gaussians. We used the objective disparities (or orientations) between the segments that were perceptually aligned (or parallel to one another) to estimate the horizontal, the vertical, and the torsional vergence. We then used the estimated vergence angles to correct the corresponding-point data. We had to assume that vergence was constant across sessions; this appeared to be a valid assumption because observer responses did not appear to drift during the course of a session and were similar between sessions.

There is no known procedure for estimating torsional version from psychophysical measurements, so we did not correct the data for this. Torsional version drifts during extended fixation, but its standard deviation is only $\sim 0.3^\circ$ (Van Rijn et al., 1994). Furthermore, torsional version in a haploscope affects each eye's projection equally, so a versional change does not affect the angular difference in projection; rather it affects the location of the eyes' targets equally. Assuming that the pattern of correspondence does not change significantly with small variations in retinal position (torsion of 0.3° produces a retinal shift of $\sim 0.04^\circ$ at the largest eccentricity we tested), torsional version will have no appreciable effect on our data.

Results

Predicted patterns

Before presenting our results, it is useful to consider the expected pattern of empirical corresponding points

under different assumptions. First, suppose these points were located at geometric corresponding points on the retinas. Under that assumption, the horizontal and the vertical disparity (the 2D disparity) between empirical corresponding points would be zero everywhere. What combination of eye position and surface orientation and shape would stimulate such points? For a point in space to stimulate the same horizontal positions in the two eyes, it must lie on the Vieth–Müller circle or on the cylinder that is the vertical extension of the circle (in Fick coordinates). Thus, we can stimulate retinal points in the same horizontal positions by presenting points on the cylinder above and below fixation for a variety of viewing distances. To understand where points in space must be to stimulate the same vertical positions in the two eyes, it is helpful to consider epipolar geometry (Fig. 20.2 of Howard & Rogers, 2002). A point in space and the nodal points of the two eyes define a plane: the epipolar plane. The intersection of the epipolar plane with the two retinas produces a pair of epipolar lines, one in each eye. Any point in the epipolar plane must project to corresponding epipolar lines in the two retinas. If the eyes are in parallel gaze (i.e., fixating at infinity), epipolar lines are in the same positions in the two eyes. If the eyes are converged to fixate at a finite distance, epipolar lines above and below fixation rotate in opposite directions in the two eyes. Thus, the only way for an extended surface to stimulate the same vertical positions in the two eyes above and below the foveae is to have the eyes in parallel gaze, and with the eyes in that position, the Vieth–Müller circle has an infinite radius. In other words, the only way for points on a surface to stimulate geometric corresponding points in the two eyes is for the surface to have an infinite distance and for the eyes to fixate at infinity.

As we have seen, geometric corresponding points cannot be stimulated by a real surface at a finite distance. It is therefore interesting to consider how empirical corresponding points would have to differ from geometric points so that a near surface could stimulate those points. Suppose that empirical points were located so that they were stimulated by a frontoparallel plane at a distance of 12 cm. Figure 3A shows that surface with the eyes fixating in the middle. Figure 3B is a plot of the pattern of points in the two retinas that would be stimulated in this case. The origin represents the foveae. Azimuth and elevation are the Helmholtz coordinates of different locations in the visual field. The green and the red points represent the positions of empirical corresponding points in the left and right eyes, respectively. There would be uncrossed horizontal disparities left and right of the vertical meridian and non-zero vertical disparities at all non-meridian locations (the absolute values of the Helmholtz elevations would be greater for the left eye's points in the left visual field and for the right eye's points in the right field). As we said earlier, empirical corresponding points near the vertical meridian of the retinas are shifted horizontally

causing the slant of the vertical horopter (Helmholtz, 1925). If a slanted plane at 12 cm (Figure 3C) stimulated corresponding points, we would observe a pattern with a vertical gradient of horizontal disparity (the Helmholtz shear) as shown in Figure 3D. As in Figure 3B, there would be uncrossed horizontal disparities left and right of fixation and non-zero vertical disparities for all non-meridian locations. There would also be uncrossed horizontal disparities above fixation and crossed disparities below.

Figures 4B and 4D plot the expected Hering–Hillebrand deviation, Helmholtz shear, and the horizontal gradient of vertical disparity (which we will call the vertical-disparity shear) for the corresponding-point patterns in Figures 3B and 3D. Notice the change in the Helmholtz shear as the optimum surface becomes slanted.

Empirical corresponding points

Figure 5 shows the 49 pairs of empirical corresponding points we measured in our observers. The Hering–Hillebrand deviation is evident along the horizontal meridian in observers PRM and KMS: corresponding points left and right of the foveae have uncrossed disparities. In observer HRF, the Hering–Hillebrand deviation was essentially zero. The Helmholtz shear is evident along the vertical meridian in all three observers: uncrossed disparities above the fovea and crossed disparities below. It is difficult, however, to see if the Hering–Hillebrand deviation and Helmholtz shear persist in the remainder of the visual field. It is also difficult to see if there is any systematic variation of vertical disparity across the visual field. To determine if the Hering–Hillebrand deviation and Helmholtz shear generalized spatially and if there is a clear pattern of vertical disparity, we transformed the data from polar to Cartesian coordinates and developed summary statistics from those transformed data. We used Cartesian coordinates because the Hering–Hillebrand deviation and Helmholtz shear could be more meaningfully expressed in such coordinates. To make the polar-Cartesian transformation, we used an interpolation algorithm. We fit the six horizontal and vertical disparities along each radial meridian separately with second-order functions: $Ae^2 + Be$, where e is eccentricity along the meridian and A and B are constants. We did not have a constant term in the fitting equation in order to constrain the fits to have a zero offset at their midpoints and thereby eliminate possible discontinuities at the center where the meridians all meet. The polar-Cartesian conversion required interpolation for locations in the Cartesian grid where we did not actually collect data. The interpolated disparity was the weighted average of measured disparities at corresponding eccentricities on the two neighboring radial meridians. From those disparities in the grid, we obtained estimates of the Hering–Hillebrand deviation, Helmholtz shear, and vertical-disparity shear. We represented

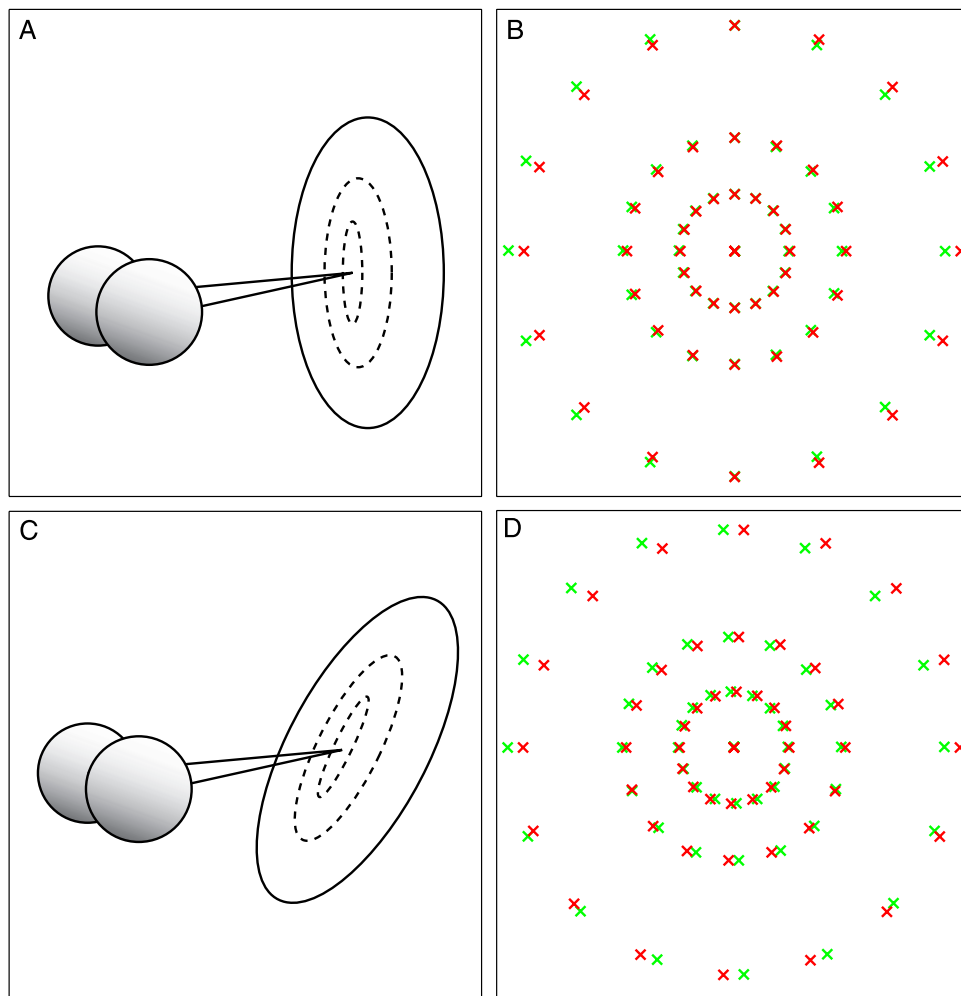


Figure 3. Predicted pattern of empirical corresponding points when the optimum surface is a plane. (A) The optimum surface is a frontoparallel plane at a distance of 12 cm. The eyes are fixated in the middle of the plane. (B) The pattern of corresponding points at the retina that would ideally be associated with that optimum surface. The foveae are superimposed in the middle of the panel. Left-eye points are represented by green symbols and right-eye points by red symbols. The horizontal position represents azimuth in Helmholtz coordinates; vertical position represents Helmholtz elevation. (C) The optimum surface is a top-back slanted plane at a distance of 12 cm. (D) The pattern of corresponding points at the retina, again in Helmholtz coordinates, that would ideally be associated with that optimum surface.

the vertical-disparity pattern in the form of a horizontal gradient because the vertical-disparity pattern of a plane viewed with symmetrical vergence is well summarized that way. The results are shown in Figures 6, 7, and 8. To estimate the error on the parameter fits, we used a bootstrapping method in which we randomly removed two points from each meridional data set before performing the fits described above. With the remaining five points (including the fixation point) on each meridian, we ran the parameter-fitting routine. We did this 50 times deriving an estimate of the Hering–Hillebrand deviation as a function of elevation, Helmholtz shear as a function of azimuth, and vertical-disparity shear as a function of elevation each time. We then used those 50 estimates to estimate the standard deviations of the fitted parameters.

We first determined the Hering–Hillebrand deviation in iso-elevation rows in Helmholtz coordinates. We started with Ogle’s (1950) formula for the Hering–Hillebrand deviation parameter H , based on relative horizontal disparities in the left and the right eyes, α_L and α_R , and the effective image magnification in the right eye relative to the left, R :

$$H = \cot \alpha_L - R \cot \alpha_R. \quad (1)$$

From this, we obtain

$$\alpha_R = \tan^{-1} \left(\frac{R \tan \alpha_L}{1 - H \tan \alpha_L} \right). \quad (2)$$

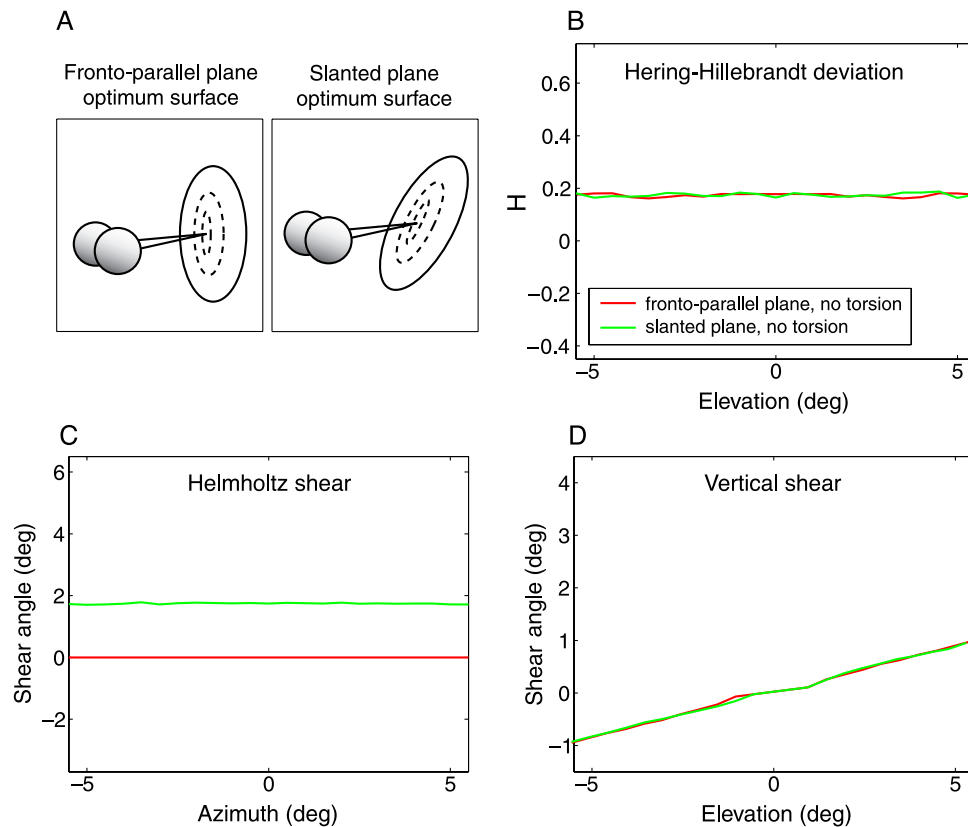


Figure 4. Predicted patterns of empirical corresponding points for an optimal planar surface at a distance of 12 cm. (A) The two viewing situations in Figure 3B. The Hering–Hillebrand deviation as a function of elevation (red for the frontoparallel plane, green for the slanted plane). The deviation is the value H in Equation 3 that provides the best fit to the horizontal disparity values at each elevation. (C) The vertical gradient of horizontal disparity (Helmholtz shear) as a function of azimuth. The shear is the angle formed between a line fit through the left eye’s corresponding points at different azimuths and a line fit through the right eye’s points at those same azimuths. (D) Horizontal gradient of vertical disparity as a function of elevation; the vertical-disparity shear. The shear is the angle formed between a line fit through the left eye points at different elevations and a line fit through the right eye’s points at the same elevations.

We can then describe the horizontal disparities D as the difference between α_L and α_R minus an elevation-specific disparity offset D_0 that we used to offset the effect of the Helmholtz shear:

$$D = \alpha_L - \tan^{-1} \left(\frac{R \tan \alpha_L}{1 - H \tan \alpha_L} \right) - D_0. \quad (3)$$

We found the values of D , H , and R that provided the best least-squares fit to the data. When $R = 1$ (equal magnification in the two eyes) and $H = D = 0$, Equation 3 describes the situation in which empirical and geometric corresponding points are the same; the empirical horopter for the horizontal meridian then becomes the Vieth–Müller circle. For $H > 0$, the horopter is less concave. We needed the parameter D_0 because the equation for the Hering–Hillebrand deviation assumes that the disparity is zero at an azimuth of zero (i.e., that $D = 0$ for $\alpha = 0$). Because of the Helmholtz shear, this assumption is false for all non-zero elevations.

We found that R did not vary with elevation, but that it was very slightly greater than 1 for all three subjects. The

slight deviation from 1 could have been caused by a very small difference in the distances of the left and right CRTs to their respective eyes.

The best H values are plotted in Figure 6. At an elevation of zero (i.e., on the horizontal meridian), H is +0.25 for observer PRM, +0.36 for KMS, and -0.11 for HRF. H is generally +0.10 to +0.30 in observers with normal binocular vision (Ogle, 1950), so the data from two of our observers are consistent with previous measurements. Of greatest interest, however, is the fact that H does not vary systematically with elevation. This result is consistent with the conclusions of Grove et al. (2001) and Ledgeway and Rogers (1999).

We also examined how the Helmholtz shear varies with azimuth. At each azimuth, we quantified the shear as the angle formed between a line fit through the left eye’s corresponding points at different elevations for a given azimuth and a line fit through the right eye’s points at that same azimuth. The shear angle as a function of azimuth is plotted in Figure 7. At an azimuth of zero, it is 2.8° for observer PRM, 6.1° for KMS, and 3.6° for HRF. Those values are consistent with previously reported values

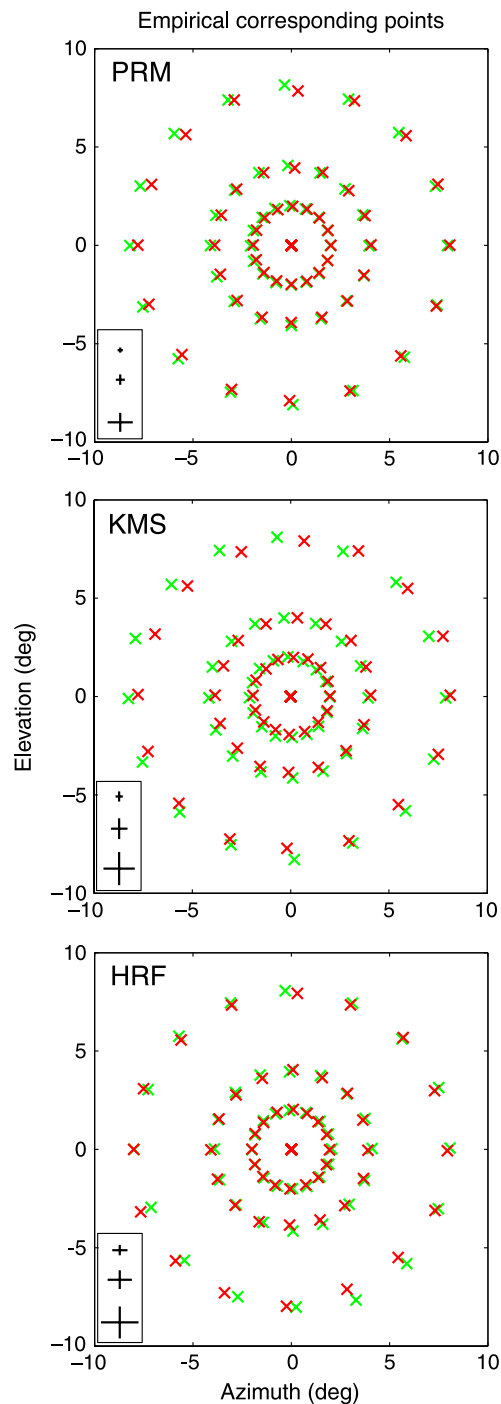


Figure 5. Empirical correspondence patterns for our three observers. The retinal locations are plotted in Helmholtz coordinates with the two retinas superimposed at the foveae and removing horizontal, vertical, and torsional eye-position offsets (see [Methods](#)). Left-eye points are green and right-eye points are red. Positive azimuth and elevation angles denote rightward and upward directions in visual space, respectively. Error bars are the black segments in the lower left of each panel. They are the average standard deviations of the probability distribution functions for the individual disparities at each eccentricity ($\pm 2^\circ$, 4° , and 8°), separate values for the horizontal and the vertical settings. They have been magnified by a factor of four for better visibility.

(Nakayama, 1977; Siderov et al., 1999). Interestingly, the shear angle varies with azimuth: It is largest at zero and decreases to the left and right of that azimuth. This means that the inclination of the horopter is greatest in the head's mid-sagittal plane. A similar shear pattern was reported by Grove et al. (2001) and Owens et al. (1987).

We also examined how the vertical disparities of empirical corresponding points vary across the visual field. We quantified the vertical-disparity shear at each elevation in essentially the same fashion that we quantified the horizontal-disparity shear at each azimuth. We fit a line through the left eye's corresponding points at each elevation and a line through the right eye's points at the same elevations. The shear angle as a function of elevation is plotted in [Figure 8](#). The shear angle was close to 0° on average, and there was no systematic change with elevation. We conclude that the vertical disparities associated with empirical corresponding points are $\sim 0^\circ$. Recall that one expects the shear angle to increase with increasing elevation if corresponding points are optimized for near viewing ([Figure 4D](#)).

Optimum surface

Having measured the retinal coordinates of empirical corresponding points for the central visual field, we turned to the problem of finding the optimum surface in space. Each corresponding-point pair generates two rays: one from the point on the left retina through the optical center of the eye into space and one from the point on the right retina into space. From our experimental measurements, we have 48 pairs of such rays. Most pairs of rays will not intersect in space, so in a simulation we moved the eyes and thereby moved the rays to find the binocular eye position for which the rays come closest to intersecting. To do this, we first found for a given eye position the point on each eye's projection ray that projects closest to the origin of the other eye's ray. We then found the point on the line connecting these two points in space that has the same angular distance from the two rays, as seen from their respective eyes. This procedure finds the point in space that projects closest in angular distance to a given pair of corresponding points. The left and the right eye's 2D disparity vectors will have the same length, but not the same direction. We defined the length of these 2D disparity vectors as the residual disparity for that pair of corresponding points. This procedure differs slightly from that used in Schreiber et al. (2006): In that paper, the points on the rays were defined not by minimal angular distance as seen from the retina, but by the minimal distance between the rays in space.

We found the binocular eye position that minimized the root mean square of residual disparities across all pairs of empirical corresponding points. In varying eye position, we held horizontal, vertical, and torsional version constant at 0° , so the simulated gaze was straight ahead. We varied horizontal, vertical, and torsional vergence simultaneously

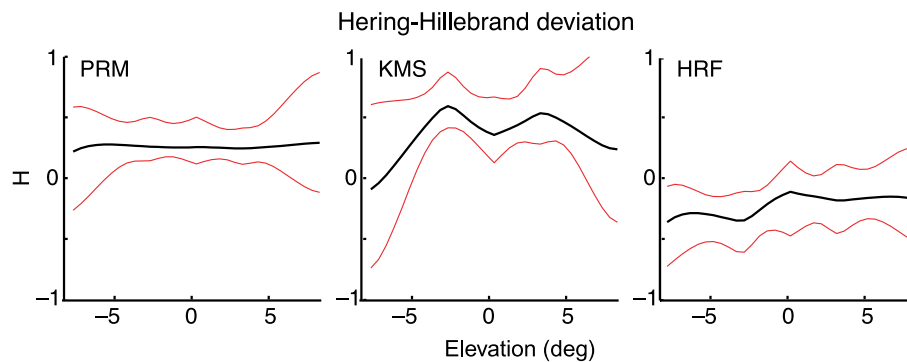


Figure 6. Best-fitting values for the Hering–Hillebrand deviation (H) as a function of elevation. The black curve is the estimated H at different elevations. The red curves represent standard deviations calculated from bootstrapping with 50 reduced data sets (Manly, 1997).

to find the combination that minimized the rms of residual disparity. The best values for the vertical and the torsional vergence were readily obtained because small variations in vergence had significant effects on the residual disparity. Small variations in the horizontal vergence had a less significant effect, but there were still best values.

The best binocular eye position for each observer is provided in Table 1. The distances at which residual disparity was minimized were 155 cm for PRM, 279 cm for KMS, and 90 cm for HRF. The fact that the best eye position was fairly distant in all observers is because the vertical disparity of corresponding points was generally $\sim 0^\circ$. Because the distances were relatively far, we conclude that empirical corresponding points are positioned for medium-range to distant viewing, and not for near viewing. Grove et al. (2001) reached a similar conclusion.

The optimum surfaces are represented by the red grids in Movie 1. Each grid intersection is the position in space that minimized the disparity of stimulated points relative to a pair of empirical corresponding points. In all three cases, the optimum surface is reasonably smooth and is slanted top-back. For observers PRM and KMS, the optimum surface is nearly planar for the eye position shown. For observer HRF, the surface is somewhat concave.

Discussion

Comparison with previous results

As we said earlier, two published studies measured empirical corresponding points across the visual field:

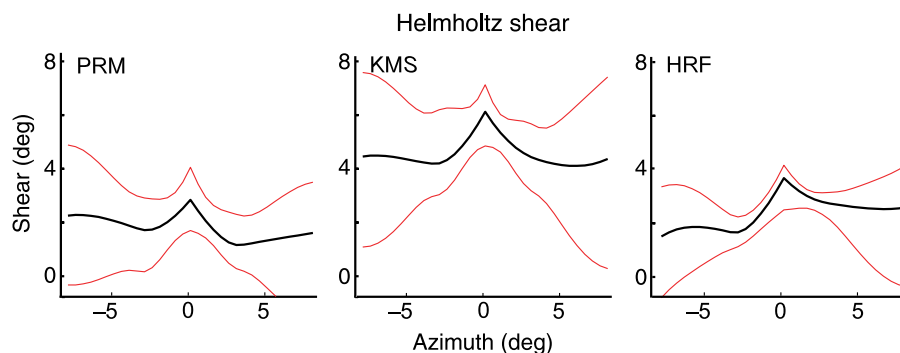


Figure 7. Best-fitting values for the Helmholtz shear (vertical gradient of horizontal disparity) as a function of azimuth. The black curves are the estimated shear at different azimuths. The red curves represent standard deviations calculated from bootstrapping (Manly, 1997). When we analyzed our data to see how the Hering–Hillebrand deviation and the Helmholtz shear generalize across the retina, we did so independently for those two disparity patterns by fitting the disparities across iso-elevation and iso-azimuth lines, respectively. While this provides reasonable descriptions of the pattern of retinal disparities, the two descriptions are not actually independent. Specifying both a Helmholtz shear value for all azimuths and the Hering–Hillebrand deviation for the visual plane (elevation zero) provides a unique value of horizontal disparity everywhere on the retina, thereby determining the values of the Hering–Hillebrand deviation at other elevations. The reverse is true when elevation-dependent Hering–Hillebrand deviations are specified together with the shear angle for the vertical meridians; this determines the shear angles for all other azimuths. Thus, Helmholtz shear and Hering–Hillebrand deviation are not independent indices of the pattern of correspondence. They are nonetheless useful descriptions of the disparity pattern across the visual field.

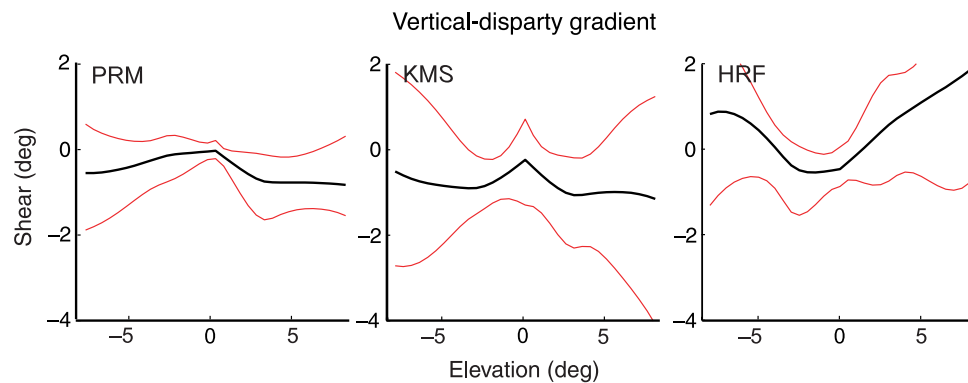


Figure 8. Best-fitting values for the vertical-disparity shear as a function of elevation. The black curve is the estimated horizontal gradient of vertical disparity (the vertical-disparity shear) at different elevations. If corresponding points were at identical locations in the two eyes, the data would be horizontal lines at a shear of 0° (Figure 4D). If corresponding points were positioned appropriately for a near surface, the data would be positively sloped lines (Figure 4D). The red curves represent standard deviations calculated from bootstrapping (Manly, 1997).

Grove et al. (2001) and Ledgeway and Rogers (1999). We next compare their results to ours.

Ledgeway and Rogers (1999)

To measure horizontal disparities associated with empirical corresponding points, Ledgeway and Rogers' (1999) observers nulled the apparent motion of two dichoptic pairs of dots: One pair was 21° above the horizontal meridian and the other was 21° below. The dot pairs were presented at azimuths from 0° to $\pm 16^\circ$. The disparity adjustments were equal and opposite for the pairs above and below the horizontal meridian. To measure the vertical disparity between corresponding points, observers adjusted the vertical disparity of two dichoptic dot pairs, one 21° to the left of the vertical meridian and the other 21° to the right. The pairs were presented at elevations from 0° to $\pm 16^\circ$, and adjustments were again equal and opposite in the pairs left and right of the vertical meridian.

	Horizontal vergence (deg)	Vertical vergence (deg)	Torsional vergence (deg)	Distance (cm)
PRM	2.40	0.01	-0.20	155
KMS	1.33	0.06	-0.53	279
HRF	4.15	0.00	-0.51	90

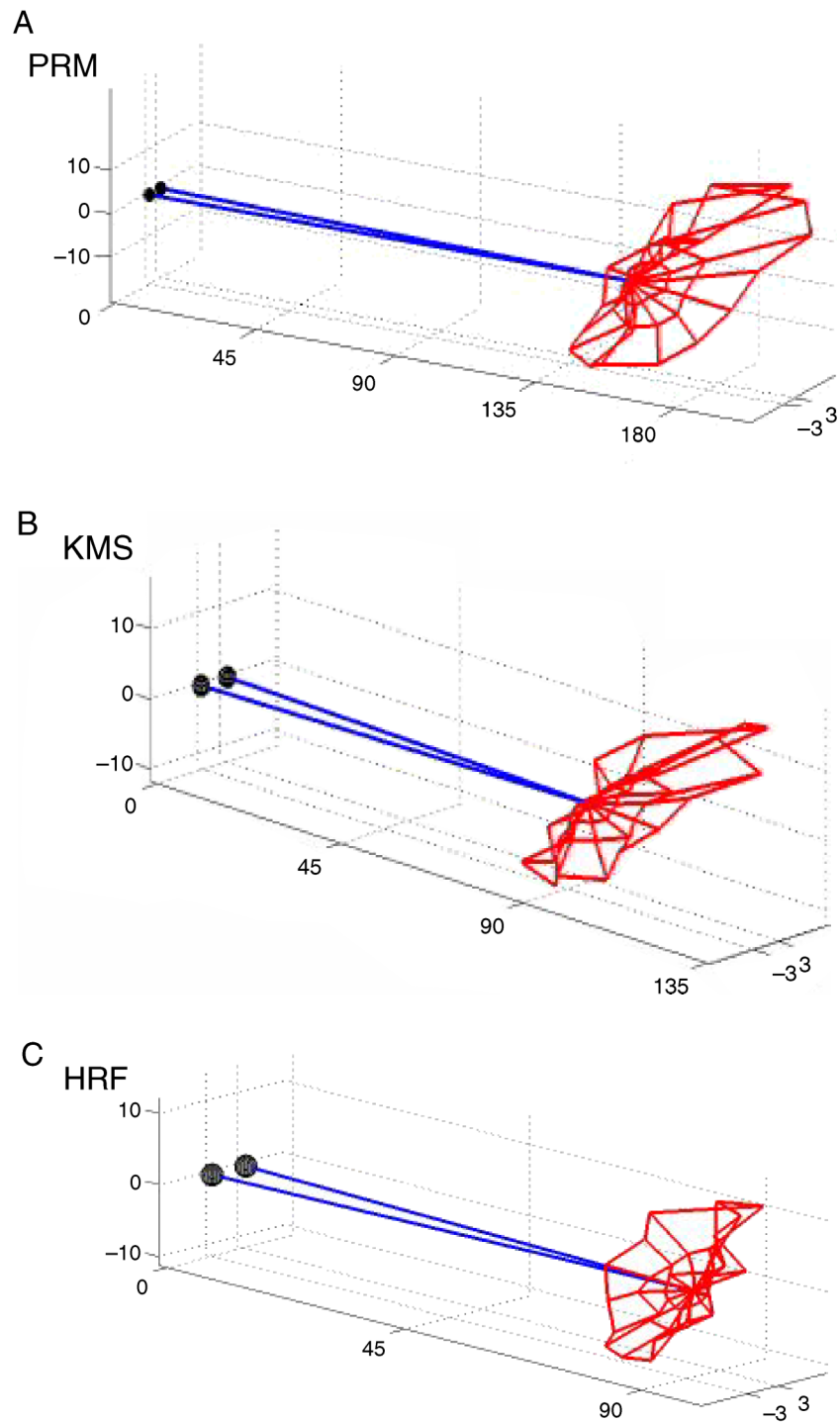
Table 1. Optimal binocular eye position for each observer. The values are the horizontal vergence, the vertical vergence, and the torsional vergence in Helmholtz coordinates that minimized the root mean square of residual disparity across the 49 pairs of empirical corresponding points. The distance corresponding to the horizontal vergence assuming an interocular distance of 6.4 cm.

Ledgeway and Rogers' (1999) method allowed them to measure horizontal and vertical disparities between corresponding points at an eccentricity of 21° , more than double the eccentricity that observers could manage in our task. However, their method assumes that horizontal and vertical disparities between corresponding points are mirror symmetric about the horizontal and the vertical meridians, respectively. As a consequence, their measurements only provide information about mirror-symmetric horizontal- and vertical-disparity shears between corresponding points. They cannot provide information about non-symmetric changes in those disparities and cannot provide information about the Hering–Hillebrand deviation (the variation of horizontal disparity with azimuth). Our measurements add to theirs because our method did not assume that the disparities between corresponding points are mirror symmetric. Thus, our measurements reveal the disparities at each visual-field location independently from disparities at other locations. Moreover, we measured disparities between corresponding points for locations closer to the foveae.

In general, our results agree with Ledgeway and Rogers' (1999). Like us, they found that the horizontal-disparity shear associated with empirical corresponding points was $4\text{--}6^\circ$ for all horizontal eccentricities. One observer (BJR) showed the same effect of azimuth that we observed—greater shear at 0° than at other azimuths—but the other two observers did not exhibit this effect. With respect to vertical disparity, Ledgeway and Rogers showed that the vertical-disparity shear between empirical corresponding points was $\sim 0^\circ$ for all elevations, and this is consistent with our observations (Figure 4D).

Grove et al. (2001)

Grove and colleagues (2001) also measured the positions of empirical corresponding points across the visual



Movie 1. The optimum surfaces for observers PRM, KMS, and HRF. The axes are in centimeters. Blue lines represent lines of sight. The red grid represents the optimal surface for that eye position. Each grid intersection is the position in space that minimizes the disparity of stimulated points with respect to one pair of empirical corresponding points. (A) Observer PRM. (B) KMS. (C) HRF. The surfaces for PRM and HRF are shown at their optimum eye positions. The optimum vergence distance for KMS was 279 centimeters, and at that distance the top part of the surface becomes quite distorted rendering the plot unintelligible. Therefore, we placed his optimum surface at 80 cm to aid interpretation.

field. Unlike Ledgeway and Rogers (1999), their method provided measurements of local horizontal disparities associated with corresponding points independent of other test locations. However, they used Ledgeway and Rogers'

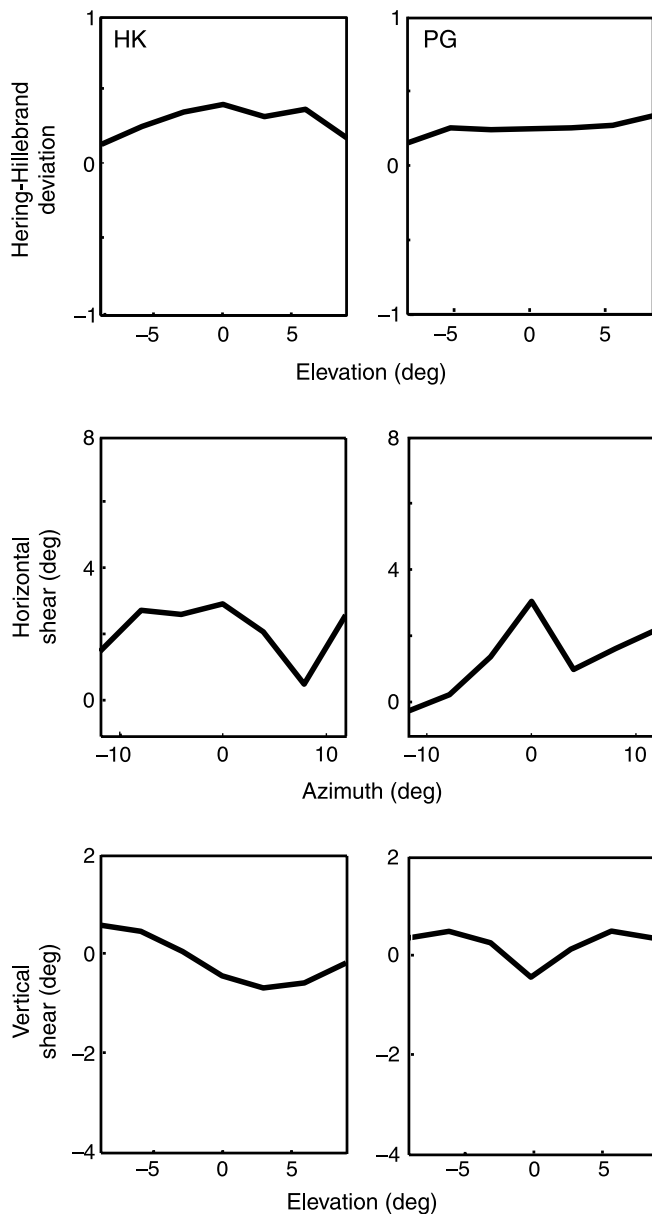


Figure 9. Best-fitting values for the data in Grove et al. (2001). The data from subjects HK and PG are in the left and the right columns, respectively. Upper row: Hering–Hillebrand deviation (H) as a function of elevation. Middle row: Helmholtz shear as a function of azimuth. Bottom row: vertical-disparity shear as a function of elevation. The data were obtained from Figure 8 of Grove et al. (2001); there were too few measurements from observer NU to run our analysis. To make the disparities in their figure more visible, Grove et al. doubled their magnitudes horizontally and vertically (Grove, personal communication, 2007); we took this magnification into account when analyzing their data.

method to measure vertical disparities, so again they could only determine the mirror-symmetric vertical shear associated with corresponding points. We subjected their data to the same analysis as ours. In particular, we determined H , the Helmholtz shear, and vertical-disparity shear for two of their three observers (the third had too few measured points). The upper row of Figure 9 plots the best-fitting H as a function of elevation. Their H values were similar to ours exhibiting a tendency toward positive values and no systematic change with elevation. The middle row of Figure 9 plots the best-fitting Helmholtz shear as a function of azimuth. They observed the same effect we did: larger shear disparities at 0° than at other azimuths. The lower row plots vertical-disparity shear as a function of elevation. There was a small variation in shear with elevation: smaller values at zero elevation than at others. That pattern is not adaptive for any viewing distance (see Figure 4D). The vertical-disparity shear they observed was quite small, so their observations were similar to ours (Figure 8): they showed no substantial variation of vertical disparity with elevation.

In summary, the results from Grove et al. (2001) and Ledgeway and Rogers (1999) are generally consistent with ours. They observed, as we did, that the Helmholtz shear occurs at all azimuths. Like us, they also observed that vertical-disparity shear at different elevations is small and is thereby consistent with a fairly distant optimum surface. Grove et al. also observed, as we did, that the Hering–Hillebrand deviation occurs at all elevations.

The vertical horopter

Helmholtz (1925) claimed that the empirical vertical horopter is a top-back slanted line in the mid-sagittal plane. The slant he said is due to horizontal shear of corresponding retinal points near the eyes' vertical meridians. More recent work, including ours (Figure 7), has confirmed both claims (Cooper & Pettigrew, 1979; Grove et al., 2001; Ledgeway & Rogers, 1999; Nakayama, 1977; Siderov et al., 1999). Helmholtz proposed that the slant of the vertical horopter had adaptive value. In particular, he claimed that the horizontal shear was close to the value required for a standing observer to have the empirical horopter in the plane of the ground. We believe his proposal has been misunderstood in the intervening years. Here we will describe the misunderstanding and then what we believe he actually proposed.

Figure 10 shows the viewing situation when an upright observer gazes at infinity in a direction parallel to the ground plane. Corresponding retinal points near the vertical meridians are rotated about the line of sight by $\theta/2$ in the left eye and $-\theta/2$ in the right eye, so the left-right difference is θ . When θ is positive, as it usually is, we will refer to this correspondence shift as extorsion. The projections of the extorted retinal meridians through the

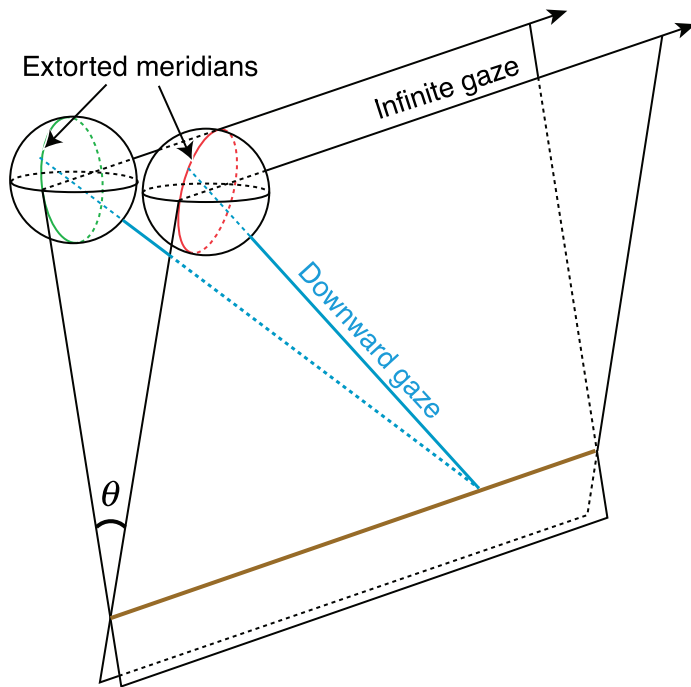


Figure 10. The viewing situation. A standing viewer with the head upright. The black lines indicate the visual axes of the eyes with gaze at an infinite distance and in a direction parallel to the ground. The green and red circles in the eyes represent the extorted corresponding meridians. The black planes are the projections of the vertical meridians through the centers of the eyes. When the meridians are extorted by θ , the planes are also extorted by θ when the eyes are in parallel gaze at infinity. The brown line is the intersection of the extorted planes; this is the empirical vertical horopter. The blue lines are the visual axes when the viewer fixates a near point at the intersection of the extorted planes. If the eyes' axes of rotation for getting from infinite to near and downward gaze are perpendicular to the great circles of the extorted meridians in the respective eyes, the extorted planes will remain stationary in head-centric coordinates.

centers of the eyes are extorted planes. The two planes intersect in a line beneath the observer when θ is positive and in a line above when θ is negative. That line of intersection is the empirical vertical horopter. With the eyes gazing parallel to the ground at an infinite distance, the vertical horopter is parallel to the ground and its elevation relative to the eyes is

$$e = \frac{-i}{2 \tan(\theta/2)}, \tag{4}$$

where i is the interocular distance. This result was described by Cooper and Pettigrew (1979, their Equation 1), Helmholtz (1925), Howard and Rogers (2002, chap. 15, their Equation 9), and others. If the elevation corresponds

to the observer's eye height, the empirical horopter lies in the ground with the eyes in parallel gaze. This arrangement would be advantageous because it causes the region of single vision and best stereopsis to coincide with the predominant environmental surface. The value of θ that places the horopter in the ground is

$$\theta_{\text{crit}} = 2 \tan^{-1}(i/2h), \tag{5}$$

where h is eye height. For heights and interocular distances that are common for humans ($h = 160$ cm; $i = 6.5$ cm), θ_{crit} is 2.32° , a value that is reasonably consistent with empirical observation (Grove et al., 2001; Helmholtz, 1925; Nakayama, 1977; our data in Figure 7). Helmholtz described this result:

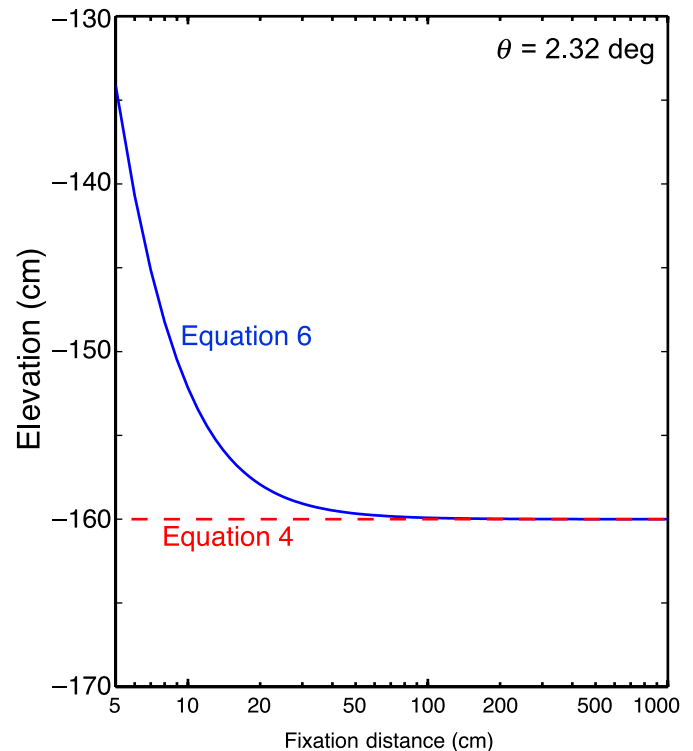


Figure 11. Elevation of the vertical horopter as it crosses under the eyes. The height of the horopter relative to the eyes is plotted as a function of fixation distance. The observer is fixating in the mid-sagittal plane in a direction parallel to the ground. For an observer with an eye height of 160 cm and interocular distance of 6.5 cm, the shear θ that places the horopter in the ground at long distances is 2.32° (Equation 5). The red curve shows the elevation predicted by Equation 4, which does not take into account the consequences of changes in horizontal vergence. The equation predicts that the horopters for different fixation distance intersect at a point: the observer's feet. The blue curve shows the elevation predicted by Equation 6, which does take horizontal vergence into account. The horopters for different fixation distances do not intersect in a point underneath the eyes.

“In one single instance the horopter is a surface, which in fact is a plane; and that is when the point of fixation is in the median plane and at an infinite distance, and the retinal horizons, as is usually the case or practically so at any rate if the eyes are normal, are both in the visual plane. Then this horopter-plane will be parallel to the visual plane, its distance from the latter depending on the amount of divergence of the apparently vertical meridians of the visual globes of the two eyes; that is, it will contain the line of intersection of these two median planes and will usually be practically the same as the horizontal plane on which the observer is standing, provided his eyes are normal and directed straight toward the horizon” (p. 424).

Since Helmholtz’s proposal, several authors have considered what happens when the eyes converge to closer distances with gaze still parallel to the ground (Cooper & Pettigrew, 1979; Nakayama, 1977, 1983; Tyler, 1991; Tyler & Scott, 1979). Because of the relationship between disparity and distance, the slant of the vertical horopter decreases with decreasing fixation distance. These authors argued from Equation 5 that when θ is constant and equal to θ_{crit} , the slant of the empirical vertical horopter varies with fixation distance such that it always runs through a point at the observer’s feet. This claim, which has been attributed to Helmholtz, is not exactly correct. To see this, reconsider Figure 10. As the eyes converge while looking parallel to the ground, they rotate about vertical axes. The extorted planes contain the fixation axes, so the planes rotate with the eyes (not shown in the figure). As a consequence, the angle between the planes changes; it is no longer θ (which is a retinal entity). The elevation of the point on the horopter directly under the eyes becomes:

$$e = \frac{-i \cos(\mu/2)}{2 \tan(\theta/2)}, \quad (6)$$

where μ is the horizontal vergence, the angle between the lines of sight. (To see this, note that the planes rotate inward when the eyes converge. The point on the horopter directly under the eyes was rotated there from a position at coordinates $(\sin(\mu/2)(i/2), \cos(\mu/2)(i/2))$ under parallel gaze. The elevation of points on the black planes in Figure 10 changes linearly from $-i/2 \tan(\theta/2)$ to 0 over a horizontal distance of $i/2$. Equation 6 follows directly. Thus, for a fixed θ , the elevation at which the vertical horopter crosses under the observer depends on fixation distance, an observation that is inconsistent with several figures in the literature (e.g., Fig. 10 in Cooper & Pettigrew, 1979; Fig. 15.29 in Howard & Rogers, 2002; Fig. 5 in Nakayama, 1977; Fig. 16.9 in Nakayama, 1983). Figure 11 shows the variation of e with fixation distance when θ is constant at θ_{crit} . The differences between

elevations predicted by Equations 4 and 6 are very small until the fixation distance becomes less than 50 cm, so the error in previous work has little practical significance.

We believe, however, that Helmholtz’s proposal about near fixations was different than the one described by modern authors. In particular, we think he was considering the position of the vertical horopter when the observer fixates in the ground plane rather than along a line at eye height parallel to the ground (e.g., Fig. 15.29; Howard & Rogers, 2002). In a brief and somewhat obscure passage, he said

“Another matter that must be mentioned here is that, when a person holds his body and head erect and looks at a point on the floor-plane which is also in the median plane of the head, the entire floor-plane is not the horopter in this case, but yet the entire rectilinear part of the horopter does lie in this plane” (p. 425).

In the context of other text in that section of the book, we believe Helmholtz was saying the following. For him the rectilinear part of the horopter was the vertical horopter. As we noted earlier, he realized that when the eyes fixate at infinity in a direction parallel to the ground (Figure 10), there is a value of θ that places the empirical vertical horopter in the ground plane. He was then considering the eye movements that would take fixation from infinity to near points in the ground and mid-sagittal plane; these movements contain a horizontal component (to converge to a shorter distance) and a vertical component (to place fixation low enough to hit the ground). There is an eye movement that would not alter the head-centric position and orientation of the extorted planes projected from the sheared vertical meridians and therefore would keep the horopter in the same head-centric location: The rotation axis has to be perpendicular to the tilted meridian in each eye when the eyes are in primary position. By rotating about that particular axis, an eye’s line of sight remains in the extorted plane; the eyes rotate through short angles to look at distant ground points and through large angles to look at near points. Because the extorted planes do not move relative to the head, their intersection—the empirical vertical horopter—remains precisely in the ground. Notice that the required axis is parallel to the head’s coronal plane, which means that the movement follows Listing’s law (Figure 10). Although he was not explicit in the above quotation, we think Helmholtz was referring to Listing’s movements when “a person ... looks at a point on the floor-plane” because he described such movements as normal eye movements throughout this section of the book. The eye movements considered explicitly by Cooper and Pettigrew (1979) and implicitly by other modern authors were only horizontal and did not place fixation in the ground.

We examined Helmholtz’s claim more closely by investigating how the value of the shear (θ) and the type of binocular eye movement affect the orientation of the

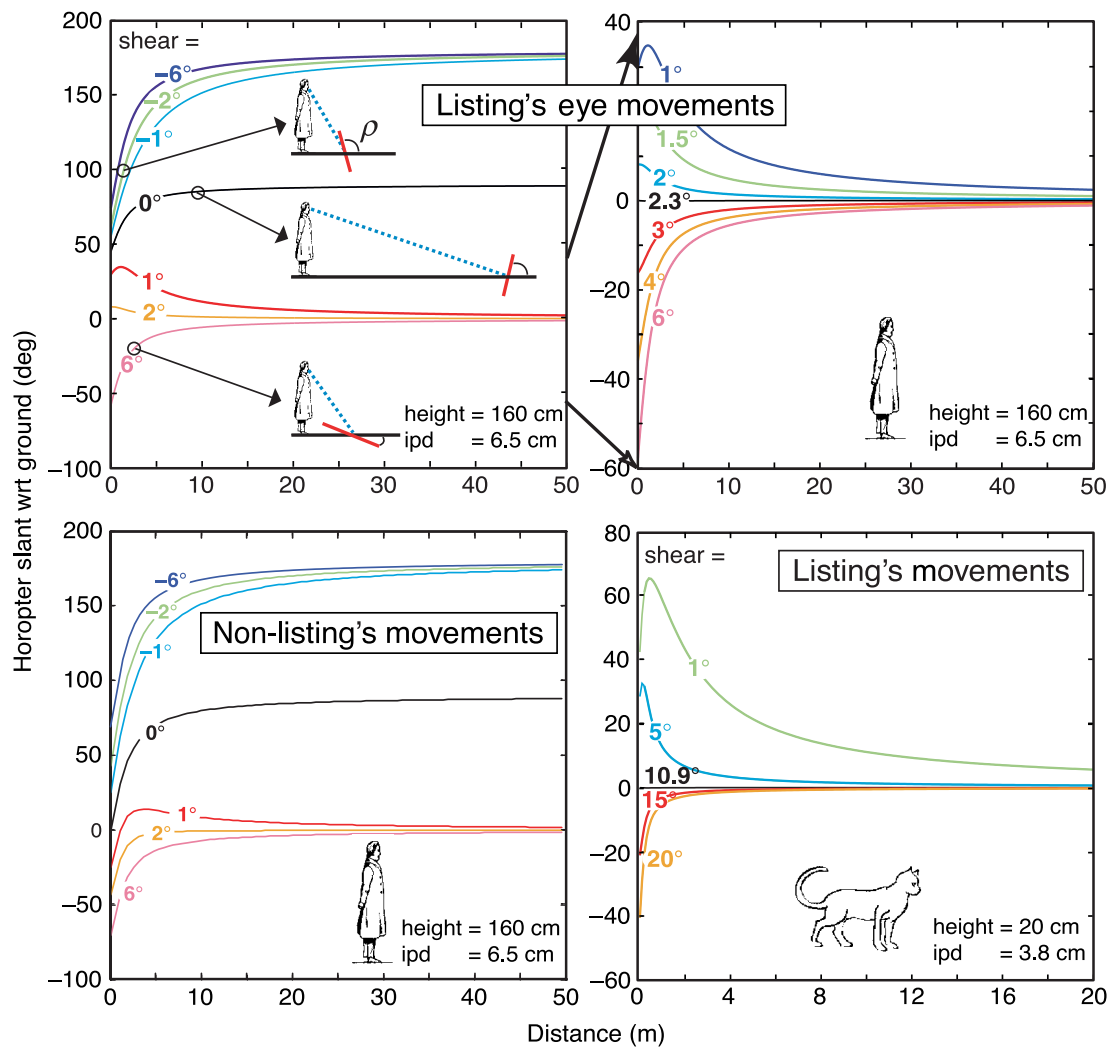


Figure 12. The relationship between fixation distance and the slant of the empirical vertical horopter with respect to the ground plane. Each panel plots the angle between the empirical horopter and the ground (ρ) as a function of the distance along the ground of the point of fixation. Upper left: eye positions following Listing's law. Each curve represents the relationship between ρ and fixation distance along the ground for a particular Helmholtz shear (θ). The insets show the viewing situation for three points. The observer's head is always upright and eye position follows Listing's law as he fixates different points in the ground. Interocular distance is 6.5 cm and eye height is 160 cm for the simulated viewer. Upper right: a magnified view of the upper left panel. ρ is exactly zero for all distances when θ is 2.32° . Lower left: Eye positions not following Listing's law but rather maintaining a Helmholtz torsion of zero in each eye. There is no value of θ that keeps the horopter in the ground at all distances, but the best value is still $\sim 2^\circ$. Lower right: Vertical horopter of the cat when eye position follows Listing's law. ρ is exactly zero for all distances when θ is 10.9° .

vertical horopter with respect to the ground. The insets in Figure 12A illustrate the viewing situation. A standing viewer with the head upright looks down to place fixation in the ground at some distance. The slant of the empirical vertical horopter (short red line segments) depends on the value of θ and the distance to the fixation point. The horopter is of course in the mid-sagittal plane. The angle between the empirical horopter and the ground is ρ , so when ρ is zero, the horopter lies in the ground. The upper two panels of Figure 12 show the relationship between θ and ρ when eye position follows Listing's law. The horopter lies precisely in the ground plane when $\theta = 2.32^\circ$

and lies close to the ground when θ is between 1.5° and 6° . The value of θ measured in different individuals nearly always falls within that range (Grove et al., 2001; Ledgeway & Rogers, 1999; Nakayama, 1977; our Figure 7). The lower left panel of Figure 12 shows the relationship between θ and ρ when eye position does not follow Listing's law. There are many such eye positions, but we show those with both eyes' Helmholtz torsion being zero. In this case, the horopter does not lie precisely in the ground plane for any value of θ , but it comes closest at a value of 2.32° and is again approximately in the ground for values between 1.5° and 6° at all but the nearest distances. Thus,

eye positions that do not obey Listing's law can still keep the horopter in the ground at all but near distances.

It is interesting to consider the vertical horopter in ground-dwelling species of different heights. Cooper and Pettigrew (1979) measured the positions of corresponding points near the vertical meridians in cat visual cortex and found an extorsion of approximately 11° , which is much greater than in humans. The lower right panel of Figure 12 shows the relationship between θ and ρ when the cat fixates in the plane of the ground with eye positions following Listing's law. The horopter lies exactly in the ground when θ is 10.9° (Equation 5) and is close for values between 5° and 20° .

In summary, we believe that Helmholtz's proposal was stronger than the modern interpretation of it. He proposed that an appropriate horizontal shear (θ_{crit}) keeps the vertical horopter in the ground as an upright viewer makes Listing's eye movements to look from one mid-sagittal location in the ground to another. This is clearly advantageous because it places the region of single vision and best stereopsis in the predominant environmental surface. Interestingly, computer-vision algorithms have adopted a similar shear for two-camera systems used to guide vehicles across the ground (Koller, Luong, & Malik, 1994).

Helmholtz's proposal involves a simplification of natural viewing. People usually fixate the ground by rotating the eyes downward relative to the head and rotating the head downward relative to the neck. Of course, the head rotation causes Listing's Planes to move so the geometry in Figure 10 is altered. A more complete account of the position of the vertical horopter relative to the ground would have to examine the contributions of head pitch and of deviations of binocular eye movements from Listing's law (Haslwanter, Straumann, Hess, & Henn, 1992; Mok et al., 1992; Nakayama, 1983; Tweed, 1997; Van Rijn & Van den Berg, 1993).

The empirical horopter and the ground plane

We showed above how a Helmholtz shear that is appropriate for a subject's interocular distance and eye height keeps the empirical vertical horopter in the ground plane for all fixations in the ground and mid-sagittal planes. We now consider the horizontal extension of the empirical horopter for fixations in the ground and the mid-sagittal planes. Thus, we need to consider not only the Helmholtz shear but also the Hering–Hillebrand deviation H that describes the curvature of the horopter relative to the Vieth–Müller circle.

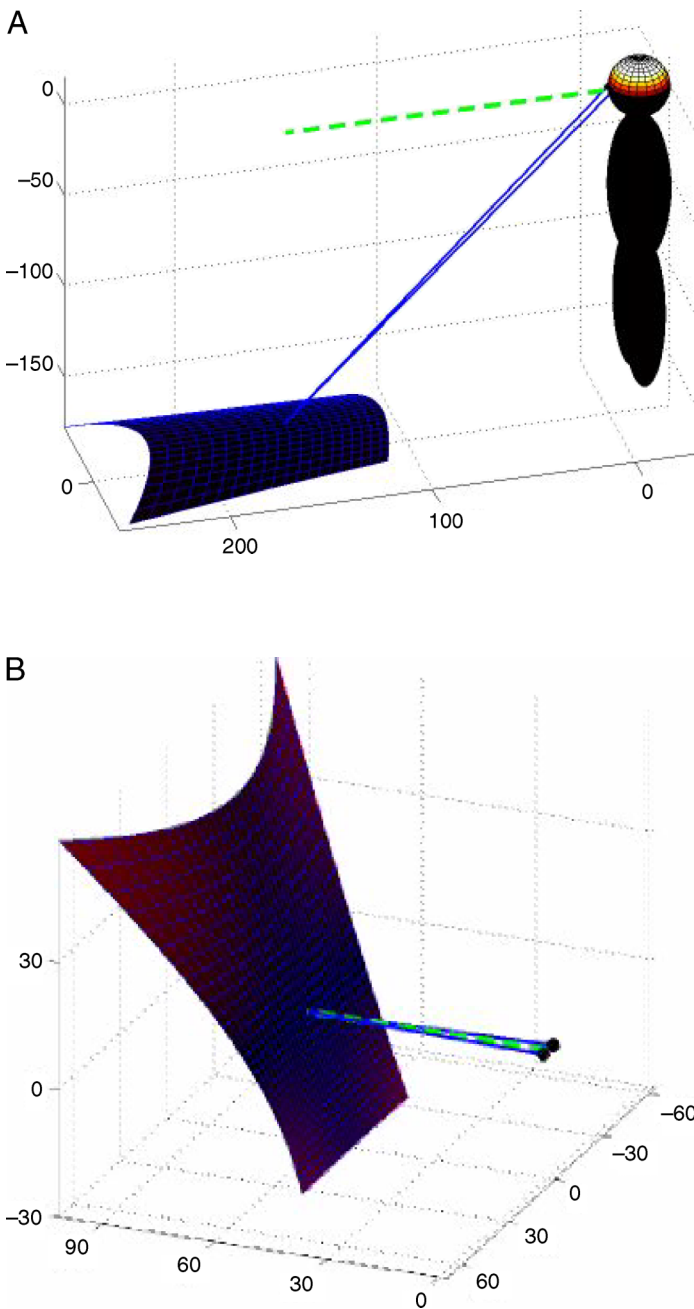
The literature suggests that the Helmholtz shear is $2\text{--}3^\circ$ on average near the vertical meridians of the eyes (Grove et al., 2001; Helmholtz, 1925; Ledgeway & Rogers, 1999; Nakayama, 1977; our Figure 8). The literature also suggests that the Hering–Hillebrand deviation H is $0.10\text{--}0.15$ on average (Ames et al., 1932; Fischer, 1924; Grove

et al., 2001; Hillis & Banks, 2001; Ledgeway & Rogers, 1999; our Figure 7). To determine how well the horizontal extension of the horopter fits the ground plane, we calculated the minimum-disparity horopter using values of 2.3° for the Helmholtz shear and 0.10 for the Hering–Hillebrand deviation. For simplicity, we assumed that the shear was the same for all azimuths and the deviation the same for all elevations; there is of course some evidence that the former assumption is slightly incorrect (Figures 8 and 9).

For a given H , the curvature of the horizontal extension of the horopter varies with distance. There is one distance—the abathic distance—at which the extension is planar. That distance is $d = i/H$, where i is interocular distance (Ogle, 1950). For distances less than the abathic distance, the extension is concave; for greater distances, it is convex. Thus, it is impossible for the horizontal extension of the horopter to be planar at all distances. Movie 2 illustrates this fact. In the left panel, a standing viewer is fixating in the ground plane and the mid-sagittal plane. The blue lines represent the two eyes' lines of sight and the green dashed line is an earth-horizontal line. The distance to the fixation point is greater than the abathic distance of 64 cm, and as a result, the horizontal extension of the horopter is convex such that it lies beneath the ground plane on the sides. The horopter surface in this case is a smooth ridge rather than a plane. The curvature of the ridge would increase with increasing fixation distance, so at long distances the horopter surface would be well below the ground on the sides. Thus, the horizontal extension of the horopter cannot in general be coincident with the plane of the ground.

Perhaps the horopter is more coincident with a nearer surface than the ground. The right panel of Movie 2 illustrates such a situation. The viewer is fixating a point above the ground at a distance corresponding to the abathic distance; again, the blue lines represent the lines of sight. For a planar surface to be nearly coincident with the horopter, it must be slanted relative to the line of sight as shown. Now the center of the horopter is planar and coincident with the surface, but the top of the horopter is concave and the bottom is convex. The changing curvature is a consequence of the interaction between the Helmholtz shear and the Hering–Hillebrand deviation. Because H is constant as a function of elevation (Figure 7 and Grove et al., 2001) and the Helmholtz shear is greater than zero (Figure 8 and many reports), the horopter has different curvatures at different elevations relative to the fixation point.

In summary, the viewing situation for which the horopter comes closest to being coincident with a planar surface is when the surface distance is equal to the abathic distance and the surface is slanted relative to the line of sight. It seems that this situation is close to the situation in normal working environments (Ankrum et al., 1995). We should point out that many previous investigators



Movie 2. (A) The minimum-disparity horopter for fixation in the ground. A standing viewer is fixating a point in the ground 160 cm forward from the feet. The blue lines represent the lines of sight, and the green dashed line is an earth-horizontal line. This analysis takes into account the Helmholtz shear and Hering–Hillebrand deviation. Assumed eye height is 160 cm, interocular distance is 6.4 cm, Helmholtz shear angle is 2.3° , and H is 0.1. (B) The minimum-disparity horopter for the same correspondence pattern with fixation at eye level at a distance of 64 cm. Again the blue lines represent the lines of sight and the dashed green line is an earth-horizontal line.

observed H values greater than the value of 0.1 that we assumed here (Ames et al., 1932; Hillis & Banks, 2001;

Ogle, 1932; Shipley & Rawlings, 1970). In those cases, the horopter comes close to being coincident with a yet nearer surface than shown in the right panel of Movie 2.

Conclusions

Our goal was to find the surface that comes closest to stimulating empirical corresponding points in the retinas. To achieve this goal, we first measured the retinal positions of empirical corresponding points for the central portion of the visual field. Those measurements showed that the Hering–Hillebrand deviation that had previously been measured along the horizontal meridian is also observed above and below that meridian. The measurements also showed that the Helmholtz shear that had previously been measured along the vertical meridian is observed left and right of the head’s mid-sagittal plane; it is largest, however, in the mid-sagittal plane. Finally, the measurements showed that there is no systematic vertical shift of empirical corresponding points relative to one another. The fact that we do not observe such shifts means that the vertical-disparity pattern is not optimized for near viewing.

With those measurements in hand, we next ran a simulation to find the binocular eye position that minimized the disparity between stimulated points relative to empirical corresponding points. There was an eye position for each observer that yielded the minimum overall disparity, but that position varied significantly across observers. Using the minimum-disparity criterion, the fixation distance corresponding to the best position was 90 to 279 cm, depending on the observer.

We also examined the coincidence between the horopter and planar surfaces when the observer fixates such surfaces. We found that the empirical vertical horopter comes very close to lying in the ground plane as the observer fixates various positions in the ground. This suggests that the Helmholtz shear of retinal correspondence may be adaptive for viewing the ground plane. The Hering–Hillebrand-deviation, on the other hand, produces a convex optimal surface that is bent out of the ground plane and is therefore unlikely to be adaptive for ground plane viewing. Using the criterion of how well the horopter surface coincides with planar surfaces, we find that the Helmholtz shear and the Hering–Hillebrand deviation are adaptive for viewing near objects that are approximately planar.

Acknowledgments

This research was supported by NIH Research Grants EY14194 (MSB) and EY03532 (CMS) and the Deutsche

Forschungsgemeinschaft. We thank Pogen MacNeilage for many hours spent as an observer and Jenny Read, Mike Landy, Greg DeAngelis, and Suzanne McKee for very helpful comments on an earlier draft. We also thank two careful reviewers whose comments improved the manuscript.

Commercial relationships: none.

Corresponding author: Kai Schreiber.

Email: kai@vision.rutgers.edu.

Current address: Aidekman Building Suite 220, 199 University Avenue, Newark, NJ 07102, USA.

References

- Ames, A., Ogle, K. N., & Gliddon, G. H. (1932). Corresponding retinal points, the horopter and size and shape of ocular images. *Journal of the Optical Society of America*, *22*, 538–631.
- Ankrum, D. R., Hansen, E. E., & Nemeth, K. J. (1995). The vertical horopter and the angle of view. In A. Gioco, G. Molteni, B. Piccoli, & E. Occhipini (Eds.), *Work with display units '94*. Amsterdam: Elsevier.
- Backus, B. T., Banks, M. S., van Ee, R., & Crowell, J. A. (1999). Horizontal and vertical disparity, eye position, and stereoscopic slant perception. *Vision Research*, *39*, 1143–1170. [PubMed]
- Badcock, D. R., & Schor, C. M. (1985). Depth-increment detection function for individual spatial channels. *Journal of the Optical Society of America A, Optics and Image Science*, *2*, 1211–1216. [PubMed]
- Blakemore, C. (1970). The range and scope of binocular depth discrimination in man. *The Journal of Physiology*, *211*, 599–622. [PubMed] [Article]
- Breitmeyer, B., Battaglia, F., & Bridge, J. (1977). Existence and implications of a tilted binocular disparity space. *Perception*, *6*, 161–164. [PubMed]
- Breitmeyer, B., Julesz, B., & Kropfl, W. (1975). Dynamic random-dot stereograms reveal up-down anisotropy and left-right isotropy between cortical hemifields. *Science*, *187*, 269–270. [PubMed]
- Brewster, D. (1844). On the law of visible position in single and binocular vision and on the representation of solid figures by the union of dissimilar plane pictures on the retina. *Transactions of the Royal Society of Edinburgh*, *15*, 349–368.
- Cooper, M. L., & Pettigrew, J. D. (1979). A neurophysiological determination of the vertical horopter in the cat and owl. *Journal of Comparative Neurology*, *184*, 1–26. [PubMed]
- Fischer, F. P. (1924). III. Experimentelle Beitrage zum Begriff der Sehrichtungsgemeinschaft der Netzhaut auf Grund der binokularen Noniusmethode. In A. Tschermak (Ed.), *Fortgesetzte Studien über Binokularsehen. Pflügers Archiv für die Gesamte Physiologie des Menschen und der Tiere*, (vol. 204, pp. 234–246).
- Flom, M. C. (1980). Corresponding and disparate retinal points in normal and anomalous correspondence. *American Journal of Optometry and Physiological Optics*, *57*, 656–665. [PubMed]
- Grove, P. M., Kaneko, H., & Ono, H. (2001). The backward inclination of a surface defined by empirical corresponding points. *Perception*, *30*, 411–429. [PubMed]
- Haslwanter, T., Straumann, D., Hess, B. J., & Henn, V. (1992). Static roll and pitch in the monkey: Shift and rotation of Listing's plane. *Vision Research*, *32*, 1341–1348. [PubMed]
- Hebbard, F. W. (1962). Comparison of subjective and objective measurements of fixation disparity. *Journal of the Optical Society of America*, *52*, 706–712.
- Helmholtz, H. (1925). *Helmholtz's treatise on physiological optics*. In J. P. C. Shouhall (Ed. & Trans.), *Handbuch der physiologischen optik* (vol. 3). New York: Optical Society of America. (Original work published 1909).
- Hillis, J. M., & Banks, M. S. (2001). Are corresponding points fixed? *Vision Research*, *41*, 2457–2473. [PubMed]
- Howard, I. P., Ohmi, M., & Sun, L. (1993). Cyclovergence: A comparison of objective and psychophysical measurements. *Experimental Brain Research*, *97*, 349–355. [PubMed]
- Howard, I. P., & Rogers, B. J. (2002). *Seeing in depth. Depth perception* (vol. 2). Ontario, Canada: I Porteous Thornhill.
- Judge, S. J., & Miles, F. A. (1985). Changes in the coupling between accommodation and vergence eye movements induced in human subjects by altering the effective interocular separation. *Perception*, *14*, 617–629. [PubMed]
- Julesz, B. (1971). *Foundations of cyclopean perception*. Chicago: University of Chicago Press.
- Koller, D., Luong, Q. T., & Malik, J. (1994). Using binocular stereopsis for vision-based vehicle control. *Proceedings of the Intelligent Vehicles '94 Symposium*, 237–242.
- Ledgeway, T., & Rogers, B. J. (1999). The effects of eccentricity and vergence angle upon the relative tilt of corresponding vertical and horizontal meridian revealed using the minimum motion paradigm. *Perception*, *28*, 143–153. [PubMed]
- Manly, B. F. J. (1997). *Randomization, Bootstrap, and Monte Carlo methodology in biology*. London: Chapman & Hall.

- Mok, D., Ro, A., Cadera, W., Crawford, J. D., & Vilis, T. (1992). Rotation of Listing's plane during vergence. *Vision Research*, *32*, 2055–2064. [[PubMed](#)]
- Nakayama, K. (1977). Human depth perception. *Society of Photo-Optical Instrumentation Engineers Journal*, *120*, 2–9.
- Nakayama, K. (1983). Kinematics of normal and strabismic eyes. In C. M. Schor, & K. J. Ciuffreda (Eds.), *Vergence eye movements: Basic and clinical aspects*. London: Butterworths.
- Ogle, K. N. (1932). An analytical treatment of the longitudinal horopter, its measurement and application to related phenomena, especially to the relative size and shape of the ocular images. *Journal of the Optical Society of America*, *22*, 665–728.
- Ogle, K. N. (1950). *Researches in binocular vision*. Philadelphia: Saunders.
- Ogle, K. N. (1953). Precision and validity of stereoscopic depth perception from double images. *Journal of the Optical Society of America*, *43*, 907–913. [[PubMed](#)]
- Owens, L. R., Kooi, F. L., & Tyler, C. W. (1987). A new twist on the vertical horopter. *Investigative Ophthalmology & Visual Science*, *28*(Suppl.), 18.
- Prince, S. J., & Eagle, R. A. (2000). Stereo correspondence in one-dimensional Gabor stimuli. *Vision Research*, *40*, 913–924. [[PubMed](#)]
- Schreiber, K. M., Tweed, D. B., & Schor, C. M. (2006). The extended horopter: Quantifying retinal correspondence across changes of 3D eye position. *Journal of Vision*, *6*(1):6, 64–74, <http://journalofvision.org/6/1/6/>, doi:10.1167/6.1.6. [[PubMed](#)] [[Article](#)]
- Schumer, R. A., & Julesz, B. (1984). Binocular disparity modulation sensitivity to disparities offset from the plane of fixation. *Vision Research*, *24*, 533–542. [[PubMed](#)]
- Shipley, T., & Rawlings, S. C. (1970). The nonius horopter. I. History and theory. *Vision Research*, *10*, 1225–1262. [[PubMed](#)]
- Siderov, J., Harwerth, R. S., & Bedell, H. E. (1999). Stereopsis, cyclovergence and the backwards tilt of the vertical horopter. *Vision Research*, *39*, 1347–1357. [[PubMed](#)]
- Tweed, D. (1997). Visual-motor optimization in binocular control. *Vision Research*, *37*, 1939–1951. [[PubMed](#)]
- Tyler, C. W. (1991). The horopter and binocular fusion (chap. 2). In D. Regan (Ed.), *Binocular vision* (pp. 19–37). Boston: CRC Press Inc.
- Tyler, C. W., & Scott, A. B. (1979). Binocular Vision. In R. E. Records (Ed.), *Physiology of the human eye and visual system*. Hagerstown: Harper & Row.
- Van Rijn, L. J., & van den Berg, A. V. (1993). Binocular eye orientation during fixations: Listing's law extended to include eye vergence. *Vision Research*, *33*, 691–708. [[PubMed](#)]
- Van Rijn, L. J., Van der Steen, J., & Collewijn, H. (1994). Instability of ocular torsion during fixation: Cyclovergence is more stable than cycloverversion. *Vision Research*, *34*, 1077–1087. [[PubMed](#)]
- Westheimer, G. (1982). The spatial grain of the perifoveal visual field. *Vision Research*, *22*, 157–162. [[PubMed](#)]
- Wichmann, F. A., & Hill, N. J. (2001). The psychometric function: I. Fitting, sampling, and goodness of fit. *Perception & Psychophysics*, *63*, 1293–1313. [[PubMed](#)] [[Article](#)]